On methane generation and decarburization in low-alloy Cr-Mo steels during hydrogen attack

Schl”gl, S.M.; van der Giessen, E.; Schlögl, Sabine M.; van Leeuwen, Yvonne

Published in:
Metallurgical and Materials Transactions A-Physical Metallurgy and Materials Science

DOI:
10.1007/s11661-000-0059-5

On Methane Generation and Decarburization in Low-Alloy Cr-Mo Steels during Hydrogen Attack

SABINE M. SCHLOGL, YVONNE VAN LEEUWEN, and ERIK VAN DER GIESSEN

Low-carbon, low-alloy Cr-Mo steels may fail by hydrogen attack when they are exposed to high hydrogen pressures at elevated temperatures. During this process, the dissolved hydrogen reacts with the carbides of the steel to form methane in grain boundary cavities. The methane pressure inside these cavities depends on the microstructure of the used steel, which consists of a ferritic matrix and alloy carbides such as M_7C_3, $M_{23}C_6$, M_6C, and M_2C. The different phases in the multicomponent system Fe-Cr-Mo-V-C are modeled with the sublattice model. Their Gibbs energies are then used to calculate the equilibrium methane pressure as a function of the microstructure. Driven by the methane pressure, the cavities grow due to grain boundary diffusion and dislocation creep, which is described by analytical relations. This leads to progressive development of damage inside the material but, at the same time, to a decrease of the carbon content in the steel. This reduction depends on, among other factors, the methane pressure and the damage state. As the carbon content also affects the creep parameters, this process of decarburization may accelerate the cavity growth. Model calculations are used to obtain insight into the influence of this decarburization process on damage evolution and the final lifetime.

I. INTRODUCTION

LOW-CARBON, low-alloy steels are often used in power plants or in the petrochemical industry. These steels mainly contain Cr, Mo, or V as significant alloying elements and their desired microstructure is a bainitic one (ferritic matrix plus alloy carbides). In case of hydrotreating and hydrocracking processes and similar applications, these steels are in contact with hydrogen and sometimes suffer from hydrogen attack (HA). This is a typical intergranular failure phenomenon caused by high hydrogen pressures at elevated temperatures. The hydrogen molecules in the gas atmosphere dissociate and the hydrogen atoms diffuse into the steel. Some get trapped at discontinuities occurring mainly between grain boundary carbides and matrix. There, the hydrogen reacts with the carbon in the steel to generate methane. The methane molecules are too large to diffuse through the steel, so they are captured inside the nucleated cavities. Consequently, an internal pressure is built up in the cavity, which drives growth of the cavity. The deformation mechanisms involved during cavity growth are grain boundary diffusion and dislocation creep. The cavities grow until coalescence, when micro cracks are formed along the grain boundaries, which link up and finally lead to intergranular failure.[1,2,3]

It has been long recognized[4] that knowing the methane pressure is of crucial importance for predicting HA lifetimes as this is the main driving force for cavity growth. The susceptibility to hydrogen attack is determined by the microstructure of the steel, especially by its alloy carbides M_xC_y. The equilibrium methane pressure can be calculated by thermodynamics. As a first approach, the activity of carbon a_C can be fitted[5] or measured.[6,7] A more insightful approach is to derive the carbon activity using the Gibbs energy of the alloy carbides. So far, only $(Cr, Fe)_3C$, $(Cr, Fe)_7C_3$, and $(Cr, Fe)_{23}C_6$ have been considered in HA models,[6,7,8] and these carbides were described by the regular solution model using the thermodynamic data given in Reference 9. The Cr-rich carbides M_7C_3 and $M_{23}C_6$ of a 2.25Cr-1Mo steel also contain Mo, which has not yet been addressed. Another missing element of these models are the Mo-rich carbides M_6C and M_2C, which also occur in 2.25Cr-1Mo.[7] Furthermore, Cr-Mo steels are often modified with V (for example, modified 2.25Cr-1Mo and modified 3Cr-1Mo), which has also not been taken into account in these HA models.

The thermodynamic data used in the former HA models are 20 years old.[9] In the meantime, sublattice models[10,11] have been established and thermodynamic parameters determined. In particular, the relevant carbide types (including the Mo-rich carbides) in the five-component system Fe-Cr-Mo-V-C have been modeled by sublattice models, and their thermodynamic parameters are available in the literature. In this article, we take the thermodynamic parameters from various sources[12–16] and use them to calculate the methane pressures for different microstructures. A further improvement over previous HA models is that we derive the partial Gibbs energies of the metals Cr, Mo, V, and Fe in the ferritic phase from a two-sublattice model for ferrite instead of simply assuming or estimating the activity coefficients for Fe, Cr, Mo, and V.

Once the equilibrium pressures are known, estimates of the HA lifetime can be made by using models to describe the growth of voids. Previous work,[3,8,17,18] however, has neglected the fact that as methane is being generated inside the cavities, the average carbon content of the steel decreases. As the C content affects the creep resistance, this process of decarburization may have an effect on the growth of a cavity and therefore on the lifetime under HA. In an attempt to quantify this effect, we exploit the information in the thermodynamic description to develop a model in

SABINE M. SCHLOGL, Postdoctoral Researcher, and ERIK VAN DER GIESSEN, Professor, Koiter Institute Delft, and YVONNE VAN LEEUWEN, Doctoral Student, Laboratory of Materials Science, are with Delft University of Technology, 2628 CD Delft, The Netherlands.

Manuscript submitted April 6, 1999.

this article that includes the influence of decarburization on cavity growth.

Section II describes how to calculate the methane pressure for different carbides. Section III gives the relations for the reduction of the carbon content as a function of methane pressure, damage state and grain size while Section IV summarizes the void growth relations used here. In Section V, the relations from Sections II through IV are applied to compute methane pressure, evolution of the carbon content, and cavity growth in various microstructures. All thermodynamic data available at this stage are summarized in the Appendix for the convenience of HA modelers.

II. METHANE PRESSURE

The methane pressure stems from the reaction of carbides with the hydrogen and depends on the various phases in the steel. In the case of an alloy carbide M_xC_y containing Cr, Mo, V, and Fe, the chemical reaction is of the type

$$(Cr_{y_{Cr}}Mo_{y_{Mo}}V_{y_V}Fe_{y_{Fe}})_xC_y + 2yH_2 \rightleftarrows yCH_4 + xy_{Cr}Cr + xy_{Mo}Mo + xy_VV + xy_{Fe}Fe \quad [1]$$

where y_{Cr}, y_{Mo}, y_V, and y_{Fe} are the concentration parameters of Cr, Mo, V, and Fe, respectively, in the carbide M_xC_y ($y_{Cr} + y_{Mo} + y_V + y_{Fe} = 1$).

The chemical reaction can be characterized by its ΔG, which is the Gibbs energy on the right-hand side minus that on the left-hand side of the reaction equation. If $\Delta G < 0$, there is a driving force for methane formation. If $\Delta G > 0$, the reactions goes in the opposite direction. If $\Delta G = 0$, the system is in equilibrium, which, in the case of Reaction [1], means that no additional methane is generated. The condition for equilibrium at a constant temperature and a constant pressure is given by

$$y\mu_{CH_4} + xy_{Cr}\mu_{Cr} + xy_{Mo}\mu_{Mo} + xy_V\mu_V + xy_{Fe}\mu_{Fe} - 2y\mu_{H_2} - \mu_{M_xC_y} = 0 \quad [2]$$

where μ_x denotes the chemical potential of the component x. The chemical potential μ_{H_2} of H_2 in the gas phase is determined by its partial pressure p_{H_2} in the following way:

$$\mu_{H_2}(p_{H_2},T) = \mu^0_{H_2}(T) + RT \ln \frac{p_{H_2}}{p^0} \quad [3]$$

or to simplify the notation,

$$\mu_{H_2} = \mu^0_{H_2} + RT \ln p_{H_2} \quad [4]$$

with $\mu^0_{H_2}$ representing the chemical potential of 1 mole H_2 in the standard state (where $p_{H_2} = p^0 = 1$ atm). Under usual hydrogen attack conditions, the methane behaves as a nonideal gas. Therefore, we express its chemical potential μ_{CH_4} in terms of the fugacity f_{CH_4} by

$$\mu_{CH_4} = \mu^0_{CH_4} + RT \ln f_{CH_4} \quad [5]$$

According to Reference 19, one can approximate the equation of state for methane through the expression

$$Z(p_{CH_4}, T) = 1 + C(T)p_{CH_4} = \frac{p_{CH_4}V_m}{RT} \quad [6]$$

for the molar compressibility $Z(p_{CH_4}, T)$, where V_m stands for the volume of one mole of methane. Then, f_{CH_4} can be directly related to the methane pressure p_{CH_4} by

$$f_{CH_4} = p_{CH_4} \exp\{C(T)p_{CH_4}\} \quad [7]$$

The values for the temperature-dependent coefficient $C(T)$ are also taken from Reference 19, and are given in the Appendix.

The metals Cr, Mo, V, and Fe do not form separate phases but are dissolved in the ferritic matrix. Therefore, we cannot simply employ their standard Gibbs energies. We have to derive the partial Gibbs energies (equivalent to the chemical potentials) of Cr, Mo, V, and Fe in the ferrite (bcc), which contains the substitutional elements Cr, Mo, and V and the interstitial alloy element C. The starting point is the Gibbs energy of the ferrite in the Fe-Cr-Mo-V-C system, which can be described with a two-sublattice model.[10] It is assumed that Fe, Cr, Mo, and V substitute each other on a metal sublattice and carbon and vacancies (Va) on an interstitial sublattice. One formula unit for bcc contains one site on the metal sublattice and three sites on the interstitial sublattice. The sublattice model yields the following Gibbs energy G^{bcc}_m for 1 mole of the formula unit $(Fe,Cr,Mo,V)(C,Va)_3$:[12–15]

$$\begin{aligned} G^{bcc}_m = {} & y_{Cr}y_{Va}\,{}^0G^{bcc}_{Cr:Va} + y_{Cr}y_C\,{}^0G^{bcc}_{Cr:C} + y_{Mo}y_{Va}\,{}^0G^{bcc}_{Mo:Va} + \\ & y_{Mo}y_C\,{}^0G^{bcc}_{Mo:C} + y_Vy_{Va}\,{}^0G^{bcc}_{V:Va} + y_Vy_C\,{}^0G^{bcc}_{V:C} + \\ & y_{Fe}y_{Va}\,{}^0G^{bcc}_{Fe:Va} + y_{Fe}y_C\,{}^0G^{bcc}_{Fe:C} + RT[y_{Cr}\ln y_{Cr} + \\ & y_{Mo}\ln y_{Mo} + y_V\ln y_V + y_{Fe}\ln y_{Fe} + \\ & 3(y_C\ln y_C + y_{Va}\ln y_{Va})] + y_{Fe}y_{Cr}(y_CL^{bcc}_{Fe,Cr:C} + \\ & y_{Va}L^{bcc}_{Fe,Cr:Va}) + y_{Fe}y_{Mo}(y_CL^{bcc}_{Fe,Mo:C} + \\ & y_{Va}L^{bcc}_{Fe,Mo:Va}) + y_{Fe}y_V(y_CL^{bcc}_{Fe,V:C} + y_{Va}L^{bcc}_{Fe,V:Va}) + \\ & y_Cy_{Va}(y_{Cr}L^{bcc}_{Cr:C,Va} + y_{Mo}L^{bcc}_{Mo:C,Va} + y_VL^{bcc}_{V:C,Va} \\ & + y_{Fe}L^{bcc}_{Fe:C,Va}) + G_{mag} \end{aligned} \quad [8]$$

The variable y_i denotes the site fraction of component i in a particular sublattice of the ferrite. The sum of the site fractions in each sublattice is defined to be equal to unity: $y_{Cr} + y_{Mo} + y_V + y_{Fe} = 1$ and $y_C + y_{Va} = 1$. ${}^0G^{bcc}_{i:Va}$ is the Gibbs energy of the pure component i in the hypothetical bcc-nonmagnetic state and ${}^0G^{bcc}_{i:C}$ is the Gibbs energy for the hypothetical bcc-nonmagnetic state where all interstitial positions are filled with carbon. The parameters $L^{bcc}_{i,j:k}$ and $L^{bcc}_{i:k,l}$ describe the mutual interaction between the elements i and j (k and l, respectively) when the other sublattice is fully occupied by the element k (i). The components on the different sublattices are separated by a colon, while the comma separates components that interact in the same sublattice. Unfortunately, not all interaction parameters are known. Therefore, in Eq. [8], only those interaction parameters are included for which data are available. The used data are given in the Appendix, together with the magnetic contribution G_{mag} to the Gibbs energy according to the model described in Reference 20. The value of G_{mag} depends on the critical temperature of magnetic ordering T_C and β, which is related to the total magnetic entropy.

From Eq. [8], we derive the partial Gibbs energies of the substitutional elements i (= Cr, Mo, V, or Fe) in ferrite as defined for a phase with several sublattices:[11]

$$\mu_i = G_m^{bcc} + \frac{\partial G_m^{bcc}}{\partial y_i} - \sum_M y_M \frac{\partial G_m^{bcc}}{\partial y_M} + \frac{\partial G_m^{bcc}}{\partial y_{Va}} - \sum_I y_I \frac{\partial G_m^{bcc}}{\partial y_I}; \quad M = \text{Cr, Mo, V, Fe} \quad I = \text{C, Va}; \qquad [9]$$

The resulting equations for μ_{Cr}, μ_{Mo}, μ_V, and μ_{Fe} are given in the Appendix in terms of y_i, ${}^0G_{i:C}$, ${}^0G_{i:Va}$, and the other thermodynamic parameters used in Eq. [8].

The Gibbs energy of the reacting carbide depends on its crystal structure, composition, and temperature. M_7C_3 can be modeled with the two-sublattice model. The first sublattice is occupied by Cr, Mo, V, and Fe (site fractions y_{Cr}, y_{Mo}, y_V, and y_{Fe}, respectively), while the second one is completely filled with carbon. If it is assumed that during HA the composition of the carbide does not change, the chemical potential of the carbide is equal to the Gibbs energy of 1 mole formula unit $(Cr_{y_{Cr}}Mo_{y_{Mo}}V_{y_V}Fe_{y_{Fe}})_7C_3$; *i.e.*[12,15]

$$\mu_{M_7C_3} = G_m^{m7c3} = y_{Cr}\,{}^0G_{Cr:C}^{m7c3} + y_{Mo}\,{}^0G_{Mo:C}^{m7c3} + y_V\,{}^0G_{V:C}^{m7c3} + y_{Fe}\,{}^0G_{Fe:C}^{m7c3} + 7RT(y_{Cr}\ln y_{Cr} + y_{Mo}\ln y_{Mo} + y_V \ln y_V + y_{Fe}\ln y_{Fe}) + y_{Cr}y_{Fe}L_{Cr,Fe:C}^{m7c3} \qquad [10]$$

$M_{23}C_6$ is modeled as a stoichiometric compound with three sublattices.[12,15] On the first sublattice, there are only sites for Cr and Fe, while on the second sublattice, one can find Cr, Mo, V, and Fe; the third sublattice is fully occupied with carbon. The Gibbs energy for $M_{23}C_6$ as well as for M_6C and the necessary thermodynamic data can be found in the Appendix. M_6C is modeled by four sublattices with an occupation ratio of 2:2:2:1.[13] The first sublattice is fully occupied by Fe, the second one by Mo, the third one by Fe, Mo, Cr, and V, and the fourth fully by carbon. The hexagonal carbide M_2C is not necessarily stoichiometric, which means that not all possible sites for carbon are actually occupied by carbon atoms. Because the M_2C carbides in the ternary subsystems Fe-Mo-C and Fe-V-C were found to be almost completely stoichiometric,[21] we treat M_2C as a stoichiometric compound with two sublattices, where the first one contains Mo, Cr, V, and Fe and the second one C.[13] More details can be found in the Appendix.

If the actual composition of the carbide and the ferritic matrix, the hydrogen pressure, and the methane pressure are known, one can substitute them together with the thermodynamic data (given in the Appendix) in Eqs. [4], [5], [9], and [10] to obtain the chemical potentials of H_2 and CH_4 in the gas phase, of Fe, Cr, Mo, and V in the solid solution ferrite, and of the carbide. Knowing these values, one can calculate ΔG, the driving force for the methane generation (Eq. [1]). The compositions of the carbides and of the ferrite of the exposed steel can be measured. As there is a surplus of hydrogen in the surrounding atmosphere and the hydrogen atoms diffuse very quickly, the partial pressure of hydrogen inside the cavity will correspond to its pressure outside. The methane pressure inside the cavities is not accessible experimentally and has to be calculated. In general, this is a formidable, coupled problem for which no solution is available at this moment. A useful approximation is obtained when one asks at which methane pressure the reaction will stop when the carbides and the ferritic matrix possess the measured composition (which may deviate from the equilibrium composition). This means that we calculate the chemical potentials (partial Gibbs energy) of Fe, Cr, Mo, and V in the ferrite and of the carbide by inserting their actual compositions into expressions [9] and [10], calculate μ_{H_2} by inserting the partial hydrogen pressure p_{H_2} into Eq. [4], assume that local equilibrium has been achieved and use the equilibrium condition [2] to determine the equilibrium methane fugacity f_{CH_4}, and with that calculate the equilibrium methane pressure p_{CH_4} from Eq. [7]. This does not necessarily mean that this methane pressure has really built up in the cavity, but we thus arrive at a conservative estimate. In this approach, we neglect kinetics and also a possible change of the composition of the ferrite due to dissolution of carbides.

For a better comparison with previous calculations of the methane pressure[5,6,7] we also use the relations mentioned previously to derive the carbon activity a_C. The chemical potential μ_C of C is given in terms of its activity a_C by

$$\mu_C = {}^0G_C^{gra} + RT\ln a_C \qquad [11]$$

where graphite (gra) is defined as the standard state of C. The term ${}^0G_C^{gra}$ stands for the Gibbs energy of 1 mole graphite at a temperature T and is equivalent to the standard chemical potential ${}^0\mu_C^{gra}$. We demonstrate the calculation of a_C for the case that the carbon comes from the carbide $(Cr_{y_{Cr}}Mo_{y_{Mo}}V_{y_V}Fe_{y_{Fe}})_7C_3$. Then, the carbon activity a_C can be calculated by

$$a_C = \exp\left(7\mu_{M_7C_3} - 7y_{Cr}\mu_{Cr} - 7y_{Mo}\mu_{Mo} - 7y_V\mu_V - 7y_{Fe}\mu_{Fe} - 3\,{}^0G_C^{gra}\right)/(3RT) \qquad [12]$$

The same procedure as mentioned previously is repeated here: computing the individual chemical potentials of Cr, Mo, V, and Fe with Eq. [9] and that of the carbide with Eq. [10] and inserting them into Eq. [12].

III. DECARBURIZATION

Hydrogen attack is a complex physical-chemical-mechanical phenomenon, involving a number of processes. Simultaneous with hydrogen diffusion and cavity nucleation, carbides dissolve and carbon atoms diffuse to the cavities where they react with the hydrogen to form methane. Due mainly to the methane pressure, the cavities grow by grain boundary diffusion and dislocation creep. It is generally assumed[2,4] that all steps involved in the methane reaction are much faster than the cavity growth process. Then, the methane pressure can be treated as being decoupled from cavity growth and p_{CH_4} can be computed as an equilibrium pressure as described in Section II. However, at least one potentially important coupling remains: due to the methane formation, the carbides partly dissolve, resulting in a decarburization of the grain material, which may significantly affect the creep resistance against cavity growth. Therefore, in this section, we consider this decarburization in closer detail.

Sufficiently many carbon atoms have to react with the hydrogen atoms to build up the equilibrium methane pressure p_{CH_4} in a cavity. The necessary amount of carbon per cavity, n_C^{cav}, is related to the volume of the cavity, V^{cav}, by $n_C^{cav} = V^{cav}/V_m$ (mol). Its mass m_C^{cav} is equal to $n_C^{cav}\,M_C$, with M_C being the molecular weight of carbon. Using Eq. [6], we can calculate m_C^{cav} as follows:

$$m_C^{cav} = \frac{p_{CH_4}\,V^{cav}\,M_C}{RT(1 + C(T)\,p_{CH_4})} \qquad [13]$$

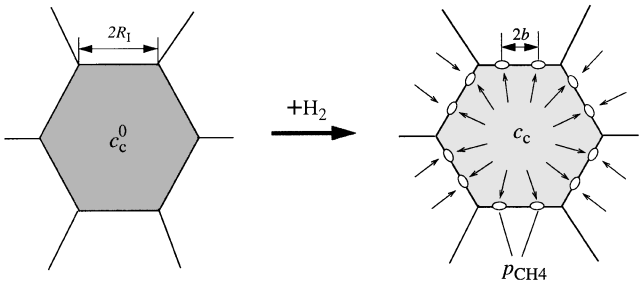

Fig. 1—Schematic view of a grain with an average facet radius of R_I before and after hydrogen attack. Its average carbon content c_C originating from carbides and ferrite is visualized by the gray scale. During HA, carbides dissolve and carbon atoms diffuse to cavities with an average spacing of 2*b*.

In the neighborhood of the cavity, some carbides dissolve and their carbon atoms diffuse through the ferritic matrix to the cavity to react with the hydrogen. Therefore, the carbon content in the neighborhood of a cavity decreases and so does the average carbon content of the grain material. Before the steel is attacked by the hydrogen (Figure 1), a grain occupying a volume V_g and total mass $m^0 = \rho V_g$ contains a certain mass of carbon, m_C^0, determined by the steel composition *c*: $m_C^0 = \rho c_C^0 V_g$ (ρ is mass density and c_C^0 the initial carbon content of the steel). If it is assumed that the grain is attacked uniformly along its facets (*cf.* References 1 and 17), the number of cavities per grain, N^{cav}, is the same on all facets and all cavities belonging to this grain have the same volume V^{cav} and the same methane pressure p_{CH_4}. The mass of the carbon atoms that have to diffuse from the grain to its facets to build up the methane pressure there is equal to $m_C^n = \frac{1}{2} N^{cav} m_C^{cav}$. Therefore, the average carbon content c_C of a uniformly attacked grain decreases to

$$c_C = \frac{m_C^0 - m_C^n}{m^0 - m_C^n} = \frac{\rho c_C^0 V_g - \frac{1}{2} N^{cav}\, m_C^{cav}}{\rho V_g - \frac{1}{2} N^{cav}\, m_C^{cav}} \qquad [14]$$

To be more specific, we approximate the shape of the grains by truncated octahedra of the same size.[22] When such a truncated-octahedral grain with an average facet radius R_I is taken to be attacked uniformly with an average half-cavity spacing *b* (Figure 1), it can be shown that the number of cavities N^{cav} of one grain and the volume of a grain V_g are related to the average facet radius R_I by the following relations:

$$N^{cav} = 14 \frac{R_I^2}{b^2} \text{ and } V_g \approx 23.8 R_I^3 \qquad [15]$$

In the results to be presented, these relations have been employed in Eq. [14] to obtain the actual carbon content of the grain.

Equations [14] and [15] show how methane pressure p_{CH_4} and cavity volume V^{cav} determine the average carbon content of a grain. Section IV will discuss how the cavity volume evolves during the HA process in response to the methane pressure, thus allowing monitoring of the accompanying decrease of the carbon content. Because the carbon content in 2.25Cr-1Mo steels significantly affects the creep properties,[23] the creep resistance will evolve during HA. As we will see subsequently, a closed-loop coupling arises because of the void growth being dependent on creep.

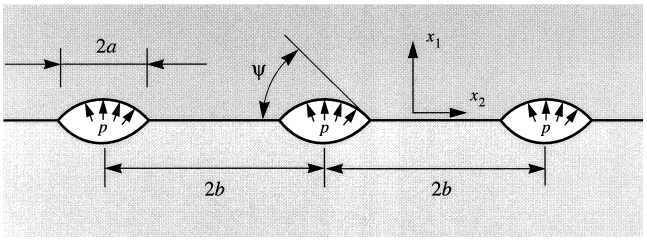

Fig. 2—Spherical cap-shaped cavities on a grain boundary facet with tip angle ψ. The radius of the cavity is *a* and its spacing to the neighboring cavity is 2*b*.

IV. VOID GROWTH RELATIONS

It has long been recognized (*e.g.*, Reference 17) that the cavities filled with the hydrogen-methane gas mixture grow by two simultaneous mechanisms: (1) surface and grain boundary diffusion and (2) creep of the grain material. Early works on HA damage[3,17,18] have essentially combined the classical Hull–Rimmer[24] model for cavity growth by grain boundary diffusion with a simple *ad hoc* correction to account for the contribution by creep. More recently, Van der Giessen *et al.*[25] have performed a more thorough analysis of void growth under internal pressure using a numerical technique to solve the coupled grain boundary diffusion-creep problem. This duly accounts for the possible interaction between creep and diffusive cavity growth due to the reduction of the diffusion path length due to local creep. They also proposed a set of approximate, yet closed-form, expressions that accurately capture their numerical solutions. These relationships have been used in the present study. The following is a brief summary for the sake of completeness; further details can be found in References 8 and 25.

For simplicity of the analysis, it is assumed that all grain boundary facets are attacked in an identical way, so that we need to consider only a single family of cavities with a radius *a*, a tip angle ψ, and a spacing of 2*b* (Figure 2). Available experimental evidence for 2.25Cr-1Mo steels shows[26] that cavities retain a near-equilibrium shape with a tip angle that is maintained at roughly the same value by virtue of surface diffusion on the inner surface of the void being much faster that grain boundary diffusion. The volume of any cavity, given by

$$V^{cav} = \frac{4}{3} \pi a^3 h(\psi),$$
$$h(\psi) = \left[(1 + \cos\psi)^{-1} - \frac{1}{2} \cos\psi \right] \Big/ \sin\psi \qquad [16]$$

is then directly related to the void size *a*, so that the rate of change of the cavity size can be immediately expressed in terms of the volumetric growth rate $\dot{V}$ according to

$$\dot{a} = \dot{V}^{cav} / (4\pi a^2 h(\psi)) \qquad [17]$$

According to Reference 25, the volumetric growth rate can be split up into a volumetric growth rate due to the diffusion of matter into the grain boundary, $\dot{V}_{diff}^{cav}$, and a contribution resulting from creep flow in the adjacent grains, $\dot{V}_{cr}^{cav}$:

$$\dot{V}^{cav} = \dot{V}_{diff}^{cav} + \dot{V}_{cr}^{cav} \qquad [18]$$

where the two contributions depend on the cavity geometry and the driving stresses for void growth.

We here consider cases only where the internal gas pressure p_m inside the cavity,

$$p_m = p_{CH_4} + p_{H_2} \quad [19]$$

presents the dominant loading state (the study in Reference 8 also accounts for the influence of additional stresses resulting from some remote loading). In this particular case, interaction between creep and diffusive contributions is negligible.[25] The volumetric growth rate due to diffusion is then given by

$$\dot{V}_{diff}^{cav} = 4\pi\mathcal{D}\,\frac{p_m - (1-f)2\gamma_s \sin\psi/a - f2T_s \sin\psi/a}{\ln(1/f) - \frac{1}{2}(3-f)(1-f)} \quad [20]$$

with $f = (a/b)^2$. Here, $\mathcal{D}$ is the temperature-dependent diffusion parameter, defined by $\mathcal{D} = D_B\delta_B\Omega/kT$ in terms of the boundary diffusivity $D_B\delta_B$ and the atomic volume Ω. The expression [20] accounts for the effects of surface energy γ_s and of surface tension T_s.

The creep contribution V_{cr}^{cav} is taken to correspond to the growth of a hole in an incompressible power-law creeping solid. That is, grain anisotropy is neglected and the grain material is assumed to behave according to the power law

$$\dot{\varepsilon} = B\sigma^n,\ B = \dot{\varepsilon}_0/\sigma_0^n \quad [21]$$

when subjected to a uniaxial stress σ. The creep exponent n is assumed to be a constant, but B is temperature dependent. Growth of a hole by creep depends sensitively on the stress triaxiality in general. In the present case of purely hydrostatic internal pressure p_m (corrected for the surface tension T_s), the volumetric growth rate expressions of Reference 8 simplify to

$$\dot{V}_{cr}^{cav} = 2\pi\dot{\varepsilon}_m a^3 h(\psi)\ \text{sign}(\sigma_m)\left[\frac{1}{1-(0.87a/b)^{3/n}}\,\alpha_n\right]^n \quad [22]$$

with

$$\sigma_m = p_m - 2T_s \sin\psi/a,\ \dot{\varepsilon}_m = B\sigma_m^n,\ \alpha_n = 3/(2n)$$

The relative contributions of diffusion and creep to void growth are conveniently weighted through the length parameter[25]

$$L_m = [\mathcal{D}p_m/\dot{\varepsilon}_m]^{1/3} \quad [23]$$

Large values of L_m compared to, for instance, the cavity spacing b indicate that growth is dominated by diffusion, while smaller values correspond to increasing contributions by creep deformations.

Following earlier work,[8,18] we assume that nucleation of the cavities takes place in the beginning of the HA process over a time scale that is much shorter than the total lifetime. Hence, the half-cavity spacing b can be taken as a constant. Given the hydrogen and methane pressure and the current cavity size a, we can then compute the instantaneous growth rate of a cavity from Eq. [17] by substitution of the volumetric growth rate expressions [18] through [22]. The complete evolution from some initial cavity radius a_I is simply obtained by time integration until a critical value of a/b at which cavity coalescence takes place (here taken to be $a/b = 0.7$).

Table I. Composition in Atomic Percent and Relative Volume Fractions of Carbides Found in Standard 2.25Cr-1Mo Steel According to Reference 7

	M_7C_3	$M_{23}C_6$	M_6C	M_2C
Average composition: Fe	35 pct	55 pct	45 pct	3 pct
Cr	60 pct	39 pct	13 pct	27 pct
Mo	5 pct	6 pct	42 pct	70 pct
Relative volume fraction	40 pct	25 pct	10 pct	25 pct

V. RESULTS

A. *Methane Pressure*

We apply the thermodynamic relations and data described in Section II and in the Appendix to calculate the methane pressure in a standard 2.25Cr-1Mo steel with bainitic microstructure at 720 K, which is about the maximum operating temperature of reactors filled with hydrogen. To obtain the methane pressure, we need the composition of the carbides and the ferritic matrix as input data. We will take advantage here of a microstructural investigation performed by Chao *et al.*[7] on standard 2.25Cr-1Mo steel with 2.5 at. pct Cr, 0.6 at. pct Mo, and 0.6 at. pct C (0.13 wt pct C). Table I shows the results of their carbide characterization. Four different types of carbides have been found in this steel, namely, M_7C_3, $M_{23}C_6$, M_6C, and M_2C. Furthermore, they measured a chromium content in the ferrite of 1.7 at. pct. Unfortunately, the molybdenum content is not reported. However, one can estimate the composition of the ferrite. Due to the low solubility of carbon in ferrite, the ferrite will contain nearly no carbon atoms, and will therefore be neglected for the sake of this analysis. First, the relative volume fractions of the carbides given in Table I are transferred into relative mole fractions by means of the volume V per metal atom of M_xC_y. We use the following values for V per metal atom: 13.75 A^3 for M_7C_3,[27] 13.13 A^3 for $M_{23}C_6$,[27,28] 18.44 A^3 for M_2C,[27,28] and 15 A^3 for M_6C (estimated). Applying these values, we obtain the following relative mole fractions of the carbides: 32 pct M_7C_3, 6 pct $M_{23}C_6$, 9 pct M_6C, and 53 pct M_2C. By knowing the mole fractions of the carbides relative to each other and their composition, one can calculate how much Cr and Mo is bounded in the carbides when all carbon of the alloy is consumed by the carbides. These amounts of Cr and Mo are then subtracted from the alloy composition. In this way, we estimate a Cr content of 1.8 at. pct and a Mo content of 0.3 at. pct. As the estimated Cr content is close to the measured one (=1.7 at. pct), we have faith in the estimated Mo content. So, the following values for the site fractions of ferrite in standard 2.25Cr-1Mo steel are substituted into Eq. [9]: $y_{Cr} = 1.7$ at. pct, $y_{Mo} = 0.3$ at. pct, and $y_C = 0.0$ at. pct.

Figure 3 shows the equilibrium methane pressures at 720 K calculated with these data for the various carbides with compositions according to Table I when they are exposed to different hydrogen pressures. Among the four different carbide types, M_7C_3 is the most unstable one, leading to a methane pressure of 210 MPa at a hydrogen pressure of 20 MPa. As explained in Section II, one can also calculate the involved carbon activity a_C. In the case of M_7C_3, we find $a_C = 0.026$, while M_6C and $M_{23}C_6$ have a carbon activity

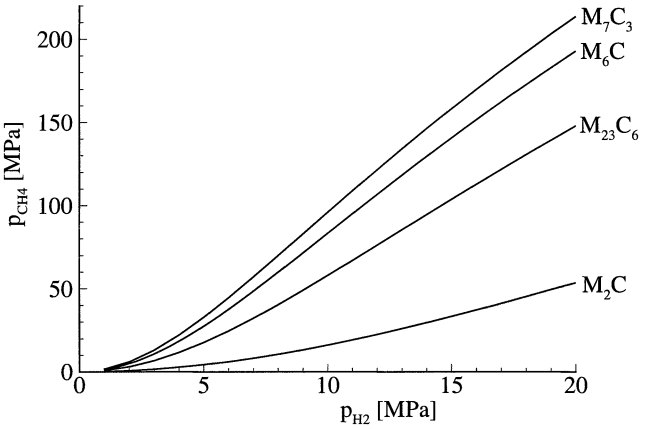

Fig. 3—Computed equilibrium methane pressure for carbides found in standard 2.25Cr-1Mo steel at 720 K. The ferrite contains 1.7 pct Cr and 0.3 pct Mo and the compositions of M_7C_3, $M_{23}C_6$, M_6C, and M_2C are given in Table I.

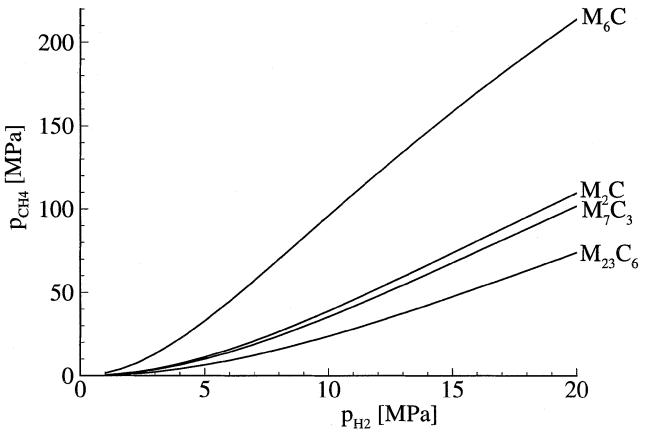

Fig. 4—Computed equilibrium methane pressure for carbides found in standard 2.25Cr-1Mo steel at 873 K. The ferrite contains 1.7 pct Cr and 0.3 pct Mo and the compositions of M_7C_3, $M_{23}C_6$, M_6C, and M_2C are given in Table I.

of 0.021 and 0.013, respectively. The lowest methane pressure is predicted for M_2C, with an activity of just 0.003.

To investigate the susceptibility to HA, autoclave tests are often performed at higher temperatures. Therefore, we repeated the calculations for 873 K and the resulting methane pressures are shown in Figure 4. Comparison with Figure 3 shows that the methane pressure decreases with increasing temperature, while the stability of the carbides relative to each other changes too. At 873 K, M_6C is the most unstable carbide ($a_C = 0.33$), followed by M_2C ($a_C = 0.10$) and M_7C_3 ($a_C = 0.09$), while $M_{23}C_6$ now gives the lowest methane pressure ($a_C = 0.06$). Chao *et al.*[7] also measured the carbon activity of their steel at 823 K and found a value of approximately 0.13. Our calculations predict similar carbon activities for a 50 deg higher temperature. Parthasarathy and Shewmon[6] investigated the carbon activities of standard 2.25Cr-1Mo steels with different tempering conditions. At 823 K, the measured activities range from 0.35 to 0.07. Nomura and Sakai[5] applied carbon activities of 0.1 and 0.04 in their model. Furthermore, they assumed the carbon activities to be temperature independent.

The resulting methane pressures are known to be quite

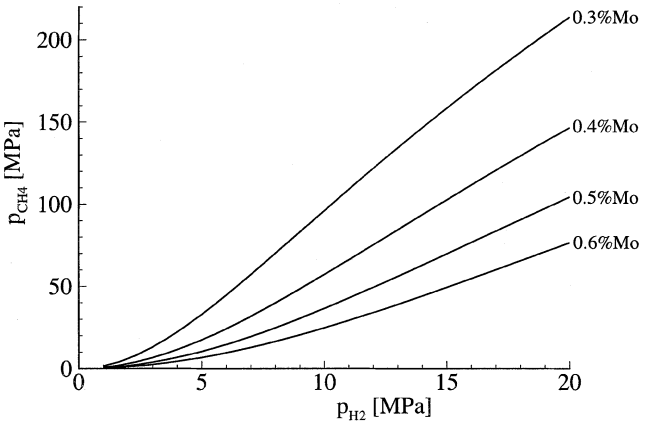

Fig. 5—Computed equilibrium methane pressure for M_6C found in standard 2.25Cr-1Mo steel at 873 K in dependence of the Mo content in the matrix. The composition of Cr in the matrix is fixed to 0.17 pct.

Table II. Composition in Atomic Percent and Relative Volume Fractions of Carbides Found in Modified 2.25Cr-1Mo Steel According to Reference 29

	M_7C_3	M_2C	MC
Average composition: Fe	33 pct	8 pct	22 pct
Cr	55 pct	18 pct	15 pct
Mo	6 pct	48 pct	19 pct
V	6 pct	26 pct	44 pct
Relative volume fraction*	75 pct	10 pct	15 pct

*Estimated.

sensitive to the composition of the ferrite,[6] especially when Mo carbides (M_6C and M_2C) are involved. Therefore, we demonstrate the effect of various Mo compositions of the ferrite for the reaction of M_6C with hydrogen at 873 K. Figure 5 shows the computed methane pressures for a ferrite with 1.7 at. pct Cr but with the Mo content varying from 0.3 to 0.6 at. pct. Due to dissolution of M_6C during HA, the Mo amount can increase from its initial value (0.3 at. pct) and approach the alloy composition 0.6 at. pct. According to Figure 5, the methane pressure at a hydrogen pressure of 20 MPa then drops from 210 to 80 MPa. Consequently, it is important to know the actual composition of the ferrite.

New steel grades are often modified with V in order to improve their resistance to HA and creep. Therefore, we study the effect of adding V to a 2.25Cr-1Mo steel on the methane pressure. A modified 2.25Cr-1Mo steel contains the carbides M_7C_3, M_2C, and MC with the composition given in Table II.[29] In the same way as described previously, we estimated the matrix composition of the modified steel with the alloy composition of 2.54 at. pct Cr, 0.6 at. pct Mo, 0.3 at. pct V, and 0.55 at. pct C. For MC, we use the value $V = 18$ A^3.[27] We then obtain the following relative mole fractions: 41 pct M_7C_3, 15 pct M_2C, and 44 pct MC, and the estimated composition of the ferrite is $y_{Cr} = 2.0$ at. pct, $y_{Mo} = 0.5$ at. pct, $y_V = 0.17$ at. pct, and $y_C = 0.0$ at. pct. Figure 6 shows the resulting methane pressure for the carbides M_7C_3 and M_2C at 720 K. Due to the addition of V, the methane pressure decreases, which can be seen when we compare Figure 6 with Figure 3. The carbon activity decreases from 0.026 to 0.017 in case of a V containing

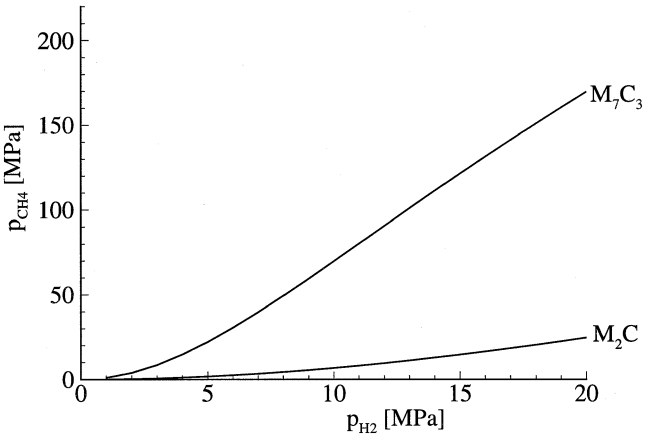

Fig. 6—Computed equilibrium methane pressure for carbides found in modified 2.25Cr-1Mo steel at 720 K. The ferrite contains 2.0 pct Cr, 0.5 pct Mo, and 0.17 pct V and the compositions of M_7C_3 and M_2C are given in Table II.

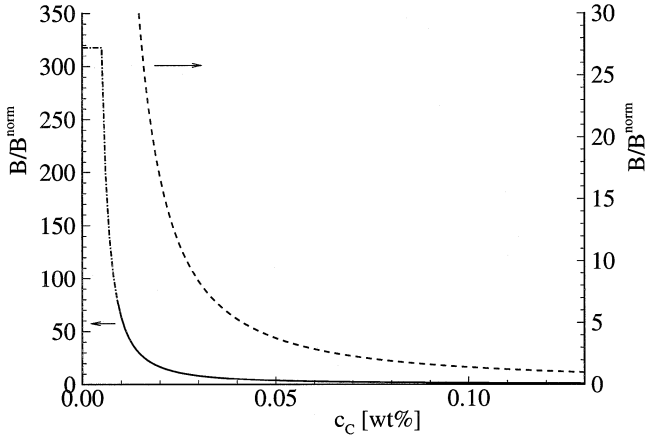

Fig. 7—Dependence of B on the carbon content c_C, normalized by the value B^{norm} at $c_C = 0.13$ wt pct. The dashed line is a blowup of the bottom regime.

M_7C_3, and from 0.003 to 0.001 for M_2C. This confirms that V improves the resistance to HA.

All results presented so far refer to the case that the ferrite possesses no carbon ($y_C = 0$). We have chosen to adopt this approximation because the ferrite possesses a low solubility of carbon and we do not know the actual value of y_C. The relationships given in Section II and in the Appendix do depend on y_C, which allows us to study the influence of y_C on the methane pressure. For $y_C = 1.5 \times 10^{-4}$, the methane pressures increase less than 5 pct compared to the ones for $y_C = 0$ presented in the Figures 3 through 6. In fact, $y_C = 1.5 \times 10^{-4}$ corresponds to 0.01 wt pct of C dissolved in ferrite, which is probably too high to be reached in the type of steels considered here.

B. *Decarburization Coupled with Void Growth*

As already explained in Section A, the methane pressure is calculated independently and serves as an input parameter in the void growth relations. We study the void growth of the standard 2.25Cr-1Mo steel with $c_C^0 = 0.13$ wt pct C at a hydrogen pressure of 18 MPa at 720 K. Under these conditions, M_7C_3 is the most unstable carbide. As shown in Figure 3, the methane pressure is 192 MPa, so that void growth is driven by an internal gas pressure p_m of 210 MPa. To be able to calculate the carbon content with Eqs. [13] and [14], we need the values of the molecular weight of carbon M_C and the density ρ of Fe; we take $M_C = 12.01$ g/mol and $\rho = 7.87 \times 10^6$ g/m^3. The cavity tip angle ψ is 78.5 deg.[3] The grain boundary diffusion parameter $\mathcal{D}(T)$ is taken as 1.32×10^{-35} m^5/(N s) at $T = 720$ K.[3] Following References 6 and 26, a value of 1 J/m^2 is used for γ_s, while T_s is taken to be 0. The creep parameters of 2.25Cr-1Mo for Eq. [22] are determined by Klueh,[23] who performed creep tests on 2.25Cr-1Mo steels with 0.009, 0.030, 0.12, and 0.135 wt pct C. We can reproduce the measured creep rates of 2.25Cr-1Mo steels for different amounts of C quite well by assuming σ_0 in Eq. [21] to depend on the logarithm of the average carbon content c_C as $\sigma_0\,(c_C) = 985.7 + 170.9 \log c_C$ (MPa), while the other parameters are kept constant: $n = 8.5$ and $\epsilon_0 = 5.5556 \times 10^{-8}$ s^{-1} at $T = 720$ K. Because only the ratio $B = \epsilon_0/\sigma_0^n$ is relevant, Figure 7 shows the used dependence of B on c_C, normalized by the value of the initial (undamaged) microstructure $B^{norm} = B(c_C^0 = 0.13$ wt pct). The dash-dotted line signifies the region ($c_C < 0.009$ wt pct) where we extrapolate beyond the experimental data of Klueh[23] by using the described function $\sigma_0(c_C)$ until values for B are reached, which are comparable to the creep data given in Reference 30.

As mentioned in Section IV, we assume that all cavities are present from the beginning. This assumption is consistent with the findings by Lopez and Shewmon[28] of the presence of submicron voids of 0.04 μm after tempering of 2.25Cr-1Mo steel. Based on this, we use a value of 0.02 μm for the initial radius of the cavities. The half-cavity spacing b ranges from 4 to 8 μm.[3] First, we investigate the damage process for the case that b is equal to 4 μm. We use the void growth relations [18] through [22] to calculate the change of the radius a with time t. While the volume of the voids increases, the carbon content in the grain decreases and the creep resistance decreases in accordance with Figure 7. According to Eqs. [14] and [15], the actual carbon content c_C of the attacked grain depends on its size, which scales with the average facet radius R_I. We vary R_I (16, 24, and 32 μm) while keeping b constant (4 μm), which leads to different degrees of decarburization resulting in different creep properties. Figure 8 shows the simultaneous time evolution of void radius a and carbon content c_C for the various R_I. The three void growth curves are signified by $B(c_C)$ to emphasize that the creep properties depend on the changing carbon content c_C. The void growth curves of $R_I = 24$ μm and of $R_I = 32$ μm almost coincide and also the one corresponding to $R_I = 16$ μm only deviates a little in the latest damage stage. Because small-grained material possesses relatively more facets, the decarburization increases with decreasing grain size, but this hardly influences the void growth. When instead, we leave the creep properties unchanged during void growth ($B = B^{norm}$), we obtain the same void growth curve as shown for $R_I = 32$ μm. In order to get a feeling for the maximum possible effect of an enhanced creep capacity due to decarburization, we repeat the analysis with creep parameters that correspond to a steel without carbon, from the beginning on. The resulting curve is referred to as $B(0)$ in Figure 8. It only deviates from the

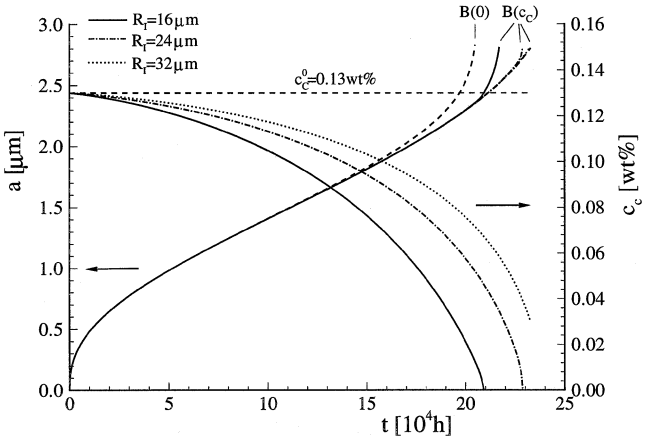

Fig. 8—Void growth of cavities with a half-spacing $b = 4\ \mu$m and evolution of the carbon content c_C for cavitated facets with an average size R_I of 16, 24, and 32 μm at 720 K due to an internal cavity pressure of 210 MPa. The curves marked by $B(c_C)$ are for cases where the creep properties depend on the current carbon content. For $B(0)$, the creep properties correspond to those of the totally decarburized steel during the entire process.

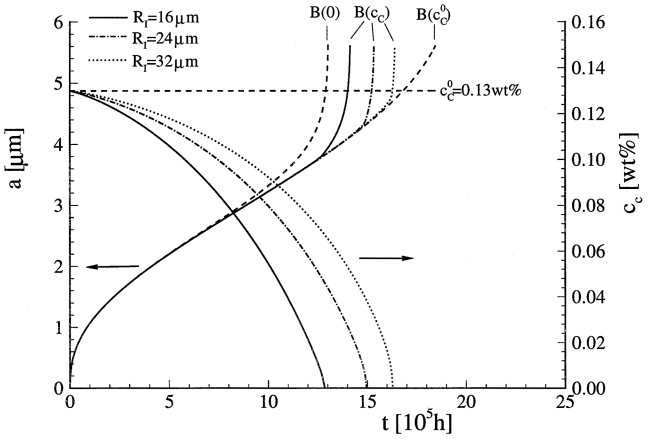

Fig. 9—Void growth of cavities with a half-spacing $b = 8\ \mu$m and evolution of the carbon content c_C for cavitated facets with an average size R_I of 16, 24, and 32 μm at 720 K due to an internal cavity pressure of 210 MPa. The curves marked by $B(c_C)$ are for cases where the creep properties depend on the current carbon content. For $B(0)$, the creep properties correspond to those of the totally decarburized steel during the entire process, while for $B(c_C^0)$, the creep properties remain the ones of the initial microstructure.

other curves near the later damage states. This tells us that cavitation is effectively dominated by grain boundary diffusion and that the deformation mechanism dislocation creep plays an unimportant role. At the early stages of cavitation, grain boundary diffusion is always the faster deformation mechanism, but, depending on the material parameters and the conditions, creep may accelerate the growth significantly during later stages. Earlier studies[8,25] have shown that cavitation is completely diffusion dominated when log $(b/L_m)$is smaller than -2 or so, while values greater than $+2$ lead to creep dominated cavitation. With the creep parameters of the initial microstructure ($c_C^0 = 0.13$ wt pct), one obtains a value of -0.01 for log (b/L_m), while it increases to 0.82 at $c_C = 0.0$ wt pct.

Figure 9 shows the result of a similar study but with a larger cavity spacing b of 8 μm. Additionally, we plot the curve $B(c_C^0)$ where the creep parameters are not updated

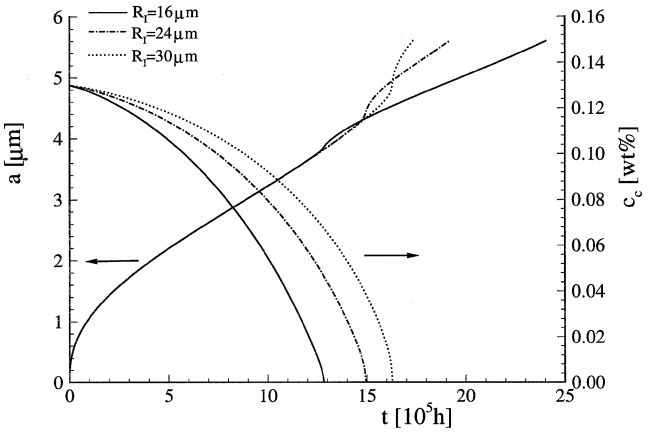

Fig. 10—Void growth of cavities with a half-spacing $b = 8\ \mu$m and evolution of the carbon content c_C for cavitated facets with an average size R_I of 16, 24, and 32 μm at 720 K due to an internal cavity pressure of 210 MPa until the carbon content is equal to zero. After total decarburization, the methane pressure is decreasing as no new methane can be generated anymore.

during void growth. Now, decarburization is more pronounced because the voids have to grow much larger before they coalesce. Due to an increase of log (b/L_m) of 0.30, creep is somewhat more important than in the previous cases, which is revealed by the difference between the two curves $B(0)$ and $B(c_C^0)$ shown in Figure 9. Therefore, the change of the creep properties according to the actual carbon content now does affect void growth, which can be seen in Figure 9. Especially, the cavities on smaller grains ($R_I = 16\ \mu$m) grow faster at a later stage of the process.

A closer look at Figure 9 reveals that accelerated growth only becomes significant after total decarburization. However, one has to be careful with the interpretation of this result because these calculations are performed with a constant cavity pressure during the entire damage process. When all the carbon of the steel has already reacted and the cavities still continue to grow, no new methane can be generated and due to the larger volume of the cavity, the methane pressure will decrease. Because we know the amount of carbon inside the cavity after total decarburization ($m_C^{cav} = 2m_C^0/N^{cav}$), we can compute the subsequent methane pressure as a function of the cavity volume by solving p_{CH_4} from Eq. [13]. Using this procedure, we have repeated the cases shown in Figure 9. The results shown in Figure 10 show that total decarburization still occurs first in the material with the small grain size, but that the rapid void growth does not continue as in Figure 9. This is caused by the fact that the methane pressure decreases quite quickly. While the cavity grows from 3.9 to 4.5 μm, the methane pressure decreases from the original 192 to 92 MPa, which significantly slows down further void growth. For larger grains, total decarburization and the decrease of the methane pressure occur at a later damage state. Then, however, the contribution of creep is higher because the creep contribution V_{cr}^{cav} in Eq. [22] scales with a^3. This is also the reason why Figure 10 predicts coalescence first for the larger grains with $R_I = 32\ \mu$m.

It follows from expressions [13] through [16] that the amount of decarburization of the grain material depends on R_I, b, and a. Figures 8 and 9 illustrate the influence of R_I at constant b. The larger the grain size, the smaller is the amount of decarburization. Because the volume increases

with the third power of R_I while N^{cav} only scales as R_I^2, c_C described by Eq. [14] increases with R_I. The influence of the half-spacing b while R_I is held fixed can be seen by comparison of Figure 8 with Figure 9. When we make the comparison for the same void radius a, a bigger spacing b leads to less decarburization because there are fewer cavities at the grain boundaries (Eqs. [14] and [15] with N^{cav} proportional to b^{-2}). When we are interested in the decarburization at the same damage state characterized by a/b, the picture changes. Then, decarburization increases with increasing b due to the fact that a is proportional with b at the same damage state (Eqs. [14] and [15] with N^{cav} m_C^{cav} proportional to $(a/b)^2 a$). It has to be noted that the expressions [13] through [16] are based on the assumption that all grain facets are cavitated homogeneously. If cavities only occur at some facets, the overall decarburization should be expected to be less. However, this cannot be quantified with the present model, because inhomogeneous cavitation requires internal stress redistribution, so that the local stress state does not need to be hydrostatic as is assumed in the void growth model in Section IV (*cf.* References 4 and 31).

VI. CONCLUSIONS

The modeling of hydrogen attack requires the knowledge of the methane pressure, which is determined by the operating conditions and by the microstructure of the steel. As Cr-Mo steels modified with V are in service in many installations, the five-component system Fe-Cr-Mo-V-C is of significant practical interest. The phases in such steels can be described with the sublattice model. The analysis in this article has used thermodynamic data of the carbides M_3C, M_7C_3, $M_{23}C_7$, M_6C, and M_2C as well as of ferrite available in the literature. Then, we have derived the relations for the chemical potentials (partial Gibbs energies) of Fe, Cr, Mo, and V in ferrite and have written them as a function of the ferrite composition in order to provide a tool for hydrogen attack modelers. The developed thermodynamic model is suitable to compute the methane pressure in standard and modified 2.25Cr-1Mo steels. The resulting equilibrium methane pressures are predicted to be quite sensitive to the carbide type and to the composition of carbide and ferrite.

The computed methane pressure for 18 MPa hydrogen pressure in standard 2.25Cr-1Mo steel at 720 K (p_{CH_4} = 192 MPa) has been employed as an input parameter in a model for void growth due to grain boundary diffusion and dislocation creep. The model developed here incorporates a conservative estimate of the influence of decarburization through its effect on the creep resistance. Decarburization is due to the continued supply of carbon atoms to the growing cavity in order to maintain the equilibrium methane pressure. This is particularly relevant during the later stages. The results, however, suggest that for a range of practically relevant material properties and conditions, decarburization has only a minor influence on cavity growth and therefore on the final lifetime.

The analyses carried out in this article are in the same spirit as most previous HA model calculations[2,4] in assuming that void growth and methane generation can be treated as decoupled processes with void growth being the rate controlling one. Kinetics, diffusion of carbon, and reduced availability of carbon for the methane formation are not accounted for. The present results suggest that this decoupling may not always be justified. In some studied cases, all the carbon available in the steel has to react to maintain the calculated equilibrium methane pressure. This implies that due to accelerated void growth before coalescence, dissolution of carbides and the reaction of C with hydrogen are required to occur very rapidly, but it is not clear if this is possible. Furthermore, the predicted severe decarburization has not been observed in standard 2.25Cr-1Mo steels. This seems to indicate that the methane pressure cannot be kept constant during void growth. Instead, dissolution of carbides, diffusion of carbon to the cavity and their reaction are likely to become controlling, especially in the later damage state. To confirm this, a much more elaborate investigation is required in which the various processes involved in hydrogen attack are considered as coupled.

APPENDIX

In this Appendix, all used thermodynamic relations and data are summarized to allow HA modelers to trace back the data easily. First, each phase φ is characterized by its Gibbs energy G_m^φ per mole of formula unit, which depends on its site fractions y_i, on the ${}^0G$ values, and on the interaction parameters L. Then, the values of ${}^0G$ and L are given in J/mol as a function of the temperature T. All numbers are in SI units with $R = 8.31451$J/(mol K). All the ${}^0G$ values are related to the enthalpy H of selected reference states for the elements at 298.15 K. This state is denoted by SER (stable element reference). Most values are taken from the literature. In cases where we could not find any references (*e.g.*, ${}^0G_{Mo:C}^{m7c3}$), we calculated the value of ${}^0G$ with MTDATA.[16] For these cases, we selected three temperatures of interest, 670, 720, and 873 K, calculated the corresponding ${}^0G$ values with MTDATA[16] and give these three values a ${}^0G$ (670 K), ${}^0G$(720 K), and ${}^0G$ (873 K).

Methane CH_4:[6,19]

Gibbs energy of formation of 1 mole CH_4:

$$\mu^0_{CH_4} - 2\mu^0_{H_2} - {}^0G_C^{gra} = -69{,}120 - 65.35T + 51.25T \log T$$

where ${}^0G_C^{gra}$ is the Gibbs energy of 1 mole graphite at a temperature T.

$$f_{CH_4} = p_{CH_4} \exp\{C(T) p_{CH_4}\}$$

with[19]

$$C(T) = 0.005 \text{ MPa}^{-1} \text{ for } f_{CH_4} < 10^3 \text{ MPa}$$

$$C(T) = \frac{1.1875}{T} + 3.0888 \times 10^{-3} \text{ MPa}^{-1}$$

$$\text{for } 10^3 < f_{CH_4} < 10^4 \text{ MPa}$$

$$C(T) = \frac{2.375}{T} + 1.1776 \times 10^{-3} \text{ MPa}^{-1}$$

$$\text{for } f_{CH_4} > 10^4 \text{ MPa}$$

Ferrite bcc:[12–15]

Two sublattices, sites 1:3

Constituents: Cr, Mo, V, Fe: C, Va

$$G_m^{bcc} = y_{Cr} y_{Va} {}^0G_{Cr:Va}^{bcc} + y_{Cr} y_C {}^0G_{Cr:C}^{bcc} + y_{Mo} y_{Va} {}^0G_{Mo:Va}^{bcc} + y_{Mo} y_C {}^0G_{Mo:C}^{bcc} + y_V y_{Va} {}^0G_{V:Va}^{bcc} + y_V y_C {}^0G_{V:C}^{bcc}$$

$$+ y_{Fe}y_{Va}\,{}^{0}G^{bcc}_{Fe:Va} + y_{Fe}y_{C}\,{}^{0}G^{bcc}_{Fe:C}$$
$$+ RT\,[y_{Cr}\ln y_{Cr} + y_{Mo}\ln y_{Mo} + y_{V}\ln y_{V}$$
$$+ y_{Fe}\ln y_{Fe} + 3(y_{C}\ln y_{C} + y_{Va}\ln y_{Va})]$$
$$+ y_{Fe}y_{Cr}\,(y_{C}L^{bcc}_{Fe,Cr:C} + y_{Va}\,L^{bcc}_{Fe,Cr:Va})$$
$$+ y_{Fe}y_{Mo}\,[y_{C}\,L^{bcc}_{Fe,Mo:C} + y_{Va}\,({}^{0}L^{bcc}_{Fe,Mo:Va}$$
$$+ {}^{1}L^{bcc}_{Fe,Mo:Va}\,(y_{Fe} - y_{Mo}))]$$
$$+ y_{Fe}y_{V}\,[y_{C}\,({}^{0}L^{bcc}_{Fe,V:C} + {}^{1}L^{bcc}_{Fe,V:C}\,(y_{Fe} - y_{V}))$$
$$+ y_{Va}\,({}^{0}L^{bcc}_{Fe,V:Va} + {}^{1}L^{bcc}_{Fe,V:Va}\,(y_{Fe} - y_{V}))]$$
$$+ y_{C}y_{Va}\,(y_{Cr}L^{bcc}_{Cr:C,Va} + y_{Mo}L^{bcc}_{Mo:C,Va} + y_{V}L^{bcc}_{V:C,Va}$$
$$+ y_{Fe}L^{bcc}_{Fe:C,Va}) + G_{mag}$$

with

$$G_{mag} = RT\ln(\beta + 1)f(\tau),\ \tau = T/T_{C}$$

for

$$\tau < 1:\ f(\tau) = -0.9053\tau^{-1} + 1.0 - 0.153\tau^{3} - 6.8\times10^{-3}\,\tau^{9} - 1.53\times10^{-3}\,\tau^{15}$$

$$T_{C} = 1043y_{Fe} - 311.5y_{Cr} + y_{Cr}y_{Fe}\,[1650 + 550(y_{Cr} - y_{Fe})] + y_{Fe}y_{Mo}\,(2y_{C} - 1)\,[335 + 526(y_{Fe} - y_{Mo})] + [-110 + 3075(y_{Fe} - y_{V}) + 808(y_{Fe} - y_{V})^{2} - 2169(y_{Fe} - y_{V})^{3}]\,y_{Fe}y_{V}(1 - y_{C})$$

$$\beta = 2.22y_{Fe}(y_{C} + y_{Va}) - 0.008y_{Cr}\,(y_{C} + y_{Va}) - 0.85y_{Cr}y_{Fe}(y_{C} + y_{Va}) - 2.26y_{Fe}y_{V}y_{Va}$$

The site fractions y_i are related to the mole fractions x_i in the following way:

$$y_{Cr} = x_{Cr}/(1 - x_{C}),\quad y_{Mo} = x_{Mo}/(1 - x_{C}),\quad y_{V} = x_{V}/(1 - y_{C})$$

$$y_{Fe} = x_{Fe}/(1 - x_{C})\quad\text{with}\quad y_{Cr} + y_{Mo} + y_{V} + y_{Fe} = 1$$

$$y_{C} = (1/3)x_{C}/(1 - x_{C})\quad\text{and}\quad y_{C} + y_{Va} = 1$$

$$\mu_{i} = G^{bcc}_{m} + \frac{\partial G^{bcc}_{m}}{\partial y_{i}} - \sum_{M} y_{M}\frac{\partial G^{bcc}_{m}}{\partial y_{M}} + \frac{\partial G^{bcc}_{m}}{\partial y_{Va}} - \sum_{I} y_{I}\frac{\partial G^{bcc}_{m}}{\partial y_{I}},$$

$$M = \text{Cr, Mo, V, Fe},\qquad I = \text{C, Va}$$

leading for $i =$ Cr, Mo, V, and Fe to the following chemical potentials μ_i (y_{Va} is substituted by $(1 - y_{C})$):

$$\mu_{Cr} = {}^{0}G^{bcc}_{Cr:Va} + y_{C}({}^{0}G^{bcc}_{Cr:C} - {}^{0}G^{bcc}_{Cr:Va}) - y_{C}\sum_{M} y_{M}\,({}^{0}G^{bcc}_{M:C} - {}^{0}G^{bcc}_{M:Va}) + RT[\ln y_{Cr} + 3\ln(y_{C} - 1)] + y_{Fe}[1 - y_{C} + y_{Cr}\,(2y_{C} - 1)]\,L^{bcc}_{Fe,Cr:Va} + y_{Fe}(1 - 2y_{Cr})\,y_{C}\,L^{bcc}_{Fe,Cr:C} + y_{Fe}y_{Mo}\,[(2y_{C} - 1)\,{}^{0}L^{bcc}_{Fe,Mo:Va} + (3y_{C} - 2)(y_{Fe} - y_{Mo})\,{}^{1}L^{bcc}_{Fe,Mo:Va} - 2y_{C}L^{bcc}_{Fe,Mo:C}] + y_{Fe}y_{V}\,[(2y_{C} - 1)\,{}^{0}L^{bcc}_{Fe,V:Va} + (3y_{C} - 2)(y_{Fe} - y_{V})\,{}^{1}L^{bcc}_{Fe,V:Va} - 2y_{C}\,{}^{0}L^{bcc}_{Fe,V:C} - 3y_{C}(y_{Fe} - y_{V})\,{}^{1}L^{bcc}_{Fe,V:C}] + y_{C}(1 - y_{C})\,L^{bcc}_{Cr:C,Va} + y_{C}(2y_{C} - 1)\sum_{M} y_{M}\,L^{bcc}_{M:C,Va} + RTf(\tau)\,[\ln(\beta + 1) + (1/(\beta + 1))(-\beta - 0.008 - 0.85y_{Fe} + 0.85y_{Cr}y_{Fe} + 2.26y_{Fe}y_{V}\,(1 - 2y_{C})]$$

$$\mu_{Mo} = {}^{0}G^{bcc}_{Mo:Va} + y_{C}({}^{0}G^{bcc}_{Mo:C} - {}^{0}G^{bcc}_{Mo:Va}) - y_{C}\sum_{M} y_{M}\,({}^{0}G^{bcc}_{M:C} - {}^{0}G^{bcc}_{M:Va}) + RT[\ln y_{Mo} + 3\ln(y_{C} - 1)] + y_{Fe}[1 - y_{C} + y_{Mo}(2y_{C} - 1)]\,{}^{0}L^{bcc}_{Fe,Mo:Va} + y_{Fe}[(1 - y_{C})(y_{Fe} - 2y_{Mo}) + y_{Mo}(y_{Fe} - y_{Mo})(3y_{C} - 2)]\,{}^{1}L^{bcc}_{Fe,Mo:Va} + y_{Fe}(1 - 2y_{Mo})y_{C}L^{bcc}_{Fe,Mo:C} + y_{Fe}y_{Cr}\,[(2y_{C} - 1)\,L^{bcc}_{Fe,Cr:Va} - 2y_{C}L^{bcc}_{Fe,Cr:C}] + y_{Fe}y_{V}\,[(2y_{C} - 1)\,{}^{0}L^{bcc}_{Fe,V:Va} + (3y_{C} - 2)(y_{Fe} - y_{V})\,{}^{1}L^{bcc}_{Fe,V:Va} - 2y_{C}\,{}^{0}L^{bcc}_{Fe,V:C} - 3y_{C}(y_{Fe} - y_{V})\,{}^{1}L^{bcc}_{Fe,V:C}] + y_{C}(1 - y_{C})\,L^{bcc}_{Mo:C,Va} + y_{C}(2y_{C} - 1)\sum_{M} y_{M}\,L^{bcc}_{M:C,Va} + RTf(\tau)[\ln(\beta + 1) + (1/(\beta + 1))(-\beta + 0.85y_{Cr}y_{Fe} + 2.26y_{Fe}y_{V}\,(1 - 2y_{C})]$$

$$\mu_{V} = {}^{0}G^{bcc}_{V:Va} + y_{C}({}^{0}G^{bcc}_{V:C} - {}^{0}G^{bcc}_{V:Va}) - y_{C}\sum_{M} y_{M}\,({}^{0}G^{bcc}_{M:C} - {}^{0}G^{bcc}_{M:Va}) + RT[\ln y_{V} + 3\ln(y_{C} - 1)] + y_{Fe}\,[1 - y_{C} + y_{V}(2y_{C} - 1)]\,{}^{0}L^{bcc}_{Fe,V:Va} + y_{Fe}[(1 - y_{C})(y_{Fe} - 2y_{V}) + y_{V}(y_{Fe} - y_{V})(3y_{C} - 2)]\,{}^{1}L^{bcc}_{Fe,V:Va} + y_{Fe}(1 - 2y_{V})y_{C}\,{}^{0}L^{bcc}_{Fe,V:C} + y_{Fe}y_{C}[(y_{Fe}(1 - 3y_{V}) + y_{V}(3y_{V} - 2)]\,{}^{1}L^{bcc}_{Fe,V:C} + y_{Fe}y_{Mo}[(2y_{C} - 1)\,{}^{0}L^{bcc}_{Fe,Mo:Va} + (3y_{C} - 2)(y_{Fe} - y_{Mo})\,{}^{1}L^{bcc}_{Fe,Mo:Va} - 2y_{C}\,L^{bcc}_{Fe,Mo:C}] + y_{Fe}y_{Cr}[(2y_{C} - 1)\,L^{bcc}_{Fe,Cr:Va} - 2y_{C}\,L^{bcc}_{Fe,Cr:C}] + y_{C}(1 - y_{C})\,L^{bcc}_{V:C,Va} + y_{C}(2y_{C} - 1)\sum_{M} y_{M}\,L^{bcc}_{M:C,Va} + RTf(\tau)[\ln(\beta + 1) + (1/(\beta + 1))(-\beta + 0.85y_{Cr}y_{Fe} - 2.26y_{Fe}(1 - y_{C}) + 2.26y_{Fe}y_{V}(1 - 2y_{C})]$$

$$\mu_{Fe} = {}^{0}G^{bcc}_{Fe:Va} + y_{C}({}^{0}G^{bcc}_{Fe:C} - {}^{0}G^{bcc}_{Fe:Va}) - y_{C}\sum_{M} y_{M}\,({}^{0}G^{bcc}_{M:C} - {}^{0}G^{bcc}_{M:Va}) + RT[\ln y_{Fe} + 3\ln(y_{C} - 1)] + y_{Cr}[1 - y_{C} + y_{Fe}(2y_{C} - 1)]\,L^{bcc}_{Fe,Cr:Va} + y_{Cr}(1 - 2y_{Fe})y_{C}\,L^{bcc}_{Fe,Cr:C} + y_{Mo}[1 - y_{C} + y_{Fe}(2y_{C} - 1)]\,{}^{0}L^{bcc}_{Fe,Mo:Va} + y_{Mo}[(1 - y_{C})(2y_{Fe} - y_{Mo}) +$$

$$y_{Fe}(y_{Fe} - y_{Mo})(3y_C - 2)]\ {}^1L^{bcc}_{Fe,Mo:Va} +$$
$$y_{Mo}(1 - 2y_{Fe})y_C\, L^{bcc}_{Fe,Mo:C} +$$
$$y_V[1 - y_C + y_{Fe}(2y_C - 1)]\ {}^0L^{bcc}_{Fe,V:Va} +$$
$$y_V[(1 - y_C)(2y_{Fe} - y_V) +$$
$$y_{Fe}(y_{Fe} - y_V)(3y_C - 2)]\ {}^1L^{bcc}_{Fe,V:Va} +$$
$$y_V(1 - 2y_{Fe})y_C\ {}^0L^{bcc}_{Fe,V:C} + y_V y_C[(y_{Fe}(2 - 3y_{Fe}) +$$
$$y_V(3y_{Fe} - 1)]\ {}^1L^{bcc}_{Fe,V:C} + y_C(1 - y_C)\, L^{bcc}_{Fe:C,Va} +$$
$$y_C(2y_C - 1)\sum_M y_M\, L^{bcc}_{M:C,Va} +$$
$$RTf(\tau)[\ln(\beta + 1) + (1/(\beta + 1))(-\beta + 2.22 +$$
$$0.85y_{Cr}(y_{Fe} - 1) - 2.26y_V(1 - y_C) +$$
$$2.26y_{Fe}y_V(1 - 2y_C)].$$

$${}^0G^{bcc}_{Fe:C} - {}^0G^{bcc}_{Fe:Va} = 3\ {}^0G^{gra}_C + 322{,}050 + 75.667T$$
$${}^0G^{bcc}_{Cr:C} - {}^0G^{bcc}_{Cr:Va} = 3\ {}^0G^{gra}_C + 416{,}000$$
$${}^0G^{bcc}_{Mo:C} - {}^0G^{bcc}_{Mo:Va} = 3\ {}^0G^{gra}_C + 331{,}000 - 75T$$
$${}^0G^{bcc}_{V:C} - {}^0G^{bcc}_{V:Va} = 3\ {}^0G^{gra}_C + 108{,}449$$
$$L^{bcc}_{Fe,Cr:Va} = 20{,}500 - 9.68T,$$
$$L^{bcc}_{Fe,Cr:C} = -1{,}750{,}000 + 940T$$
$${}^0L^{bcc}_{Fe,Mo:Va} = 36{,}818 - 9.141T,$$
$${}^1L^{bcc}_{Fe,Mo:Va} = -362 - 5.724T$$
$$L^{bcc}_{Fe,Mo:C} = -1{,}750{,}000 + 940T$$
$${}^0L^{bcc}_{Fe,V:Va} = -23{,}674 + 0.465T, \quad {}^1L^{bcc}_{Fe,V:Va} = 8283$$
$${}^0L^{bcc}_{Fe,V:C} = -23{,}674 + 0.465T, \quad {}^1L^{bcc}_{Fe,V:C} = 8283$$
$$L^{bcc}_{Fe:C,Va} = -190T, \quad L^{bcc}_{Cr:C,Va} = -190T,$$
$$L^{bcc}_{Mo:C,Va} = -190T, \quad L^{bcc}_{V:C,Va} = -297{,}868$$

Cementite:[12,15]

Two sublattices, sites 3:1
Constituents: Cr, V, Fe:C

$$G^{cem}_m = y_{Cr}\ {}^0G^{cem}_{Cr:C} + y_V\ {}^0G^{cem}_{V:C} + y_{Fe}\ {}^0G^{cem}_{Fe:C}$$
$$+ 3RT(y_{Cr}\ln y_{Cr} + y_V \ln y_V + y_{Fe}\ln y_{Fe})$$
$$+ y_{Cr}y_{Fe}\, L^{cem}_{Cr,Fe:C} + y_V y_{Fe}\, L^{cem}_{V,Fe:C}$$
$${}^0G^{cem}_{Cr:C} - 3H^{SER}_{Cr} - H^{SER}_C = 3GHSERCR$$
$$+ GHSERC - 39{,}744 - 18.08T$$
$${}^0G^{cem}_{V:C} - 3H^{SER}_V - H^{SER}_C = -156{,}971$$
$$+ 601.922T - 100.438T\ln T + 765{,}557T^{-1}$$
$${}^0G^{cem}_{Fe:C} - 3H^{SER}_{Fe} - H^{SER}_C = -10{,}745$$
$$+ 706.04T - 120.6T\ln T$$
$$L^{cem}_{Cr,Fe:C} = 29{,}260 - 16.63T$$
$$L^{cem}_{V,Fe:C} = -45{,}873 - 12.414T$$

M_7C_3:[12,15,16]

Two sublattices, sites 7:3
Constituents: Cr, Mo, V, Fe:C

$$\mu_{M_7C_3} = G^{m7c3}_m = y_{Cr}\ {}^0G^{m7c3}_{Cr:C} + y_{Mo}\ {}^0G^{m7c3}_{Mo:C}$$
$$+ y_V\ {}^0G^{m7c3}_{V:C} + y_{Fe}\ {}^0G^{m7c3}_{Fe:C} + 7RT\,(y_{Cr}\ln y_{Cr}$$
$$+ y_{Mo}\ln y_{Mo} + y_V \ln y_V + y_{Fe}\ln y_{Fe})$$
$$+ y_{Cr}\, y_{Fe}\, L^{m7c3}_{Cr,Fe:C}$$
$${}^0G^{m7c3}_{Cr:C} - 7H^{SER}_{Cr} - 3H^{SER}_C = -209{,}752$$
$$+ 980.29T - 170.5T\ln T - 0.0690921T^2$$
$${}^0G^{m7c3}_{V:C} - 7H^{SER}_V - 3H^{SER}_C = -454{,}245$$
$$+ 1518.48T - 250.981T\ln T + 2148691T^{-1}$$
$${}^0G^{m7c3}_{Fe:C} - 7H^{SER}_{Fe} - 3H^{SER}_C = 7GHSERFE$$
$$+ 3GHSERC + 113{,}385 - 78.37T$$

${}^0G^{m7c3}_{Mo:C}(T)$:[16]

$${}^0G^{m7c3}_{Mo:C}(670K) - 7H^{SER}_{Mo} - 3H^{SER}_C = -301{,}000$$
$${}^0G^{m7c3}_{Mo:C}(720K) - 7H^{SER}_{Mo} - 3H^{SER}_C = -319{,}000$$
$${}^0G^{m7c3}_{Mo:C}(873K) - 7H^{SER}_{Mo} - 3H^{SER}_C = -380{,}354$$
$$L^{m7c3}_{Cr,Fe:C} = -10{,}465$$

$M_{23}C_6$:[12,15,16]

Three sublattices called *s*, *t*, and *u*, sites 20:3:6
Constituents: Cr, Fe:Cr, Mo, V, Fe:C

$$(Cr_{y_{Cr}}Mo_{y_{Mo}}V_{y_V}Fe_{y_{Fe}})_{23}C_6$$
$$\rightarrow (Cr_{y^s_{Cr}}Fe_{y^s_{Fe}})_{20}(Cr_{y^t_{Cr}}Mo_{y^t_{Mo}}V_{y^t_V}Fe_{y^t_{Fe}})_3C_6$$
$$\mu_{M_{23}C_6} = G^{m23c6}_m = y^s_{Fe}(y^t_{Fe}\ {}^0G^{m23c6}_{Fe:Fe:C} + y^t_{Cr}\ {}^0G^{m23c6}_{Fe:Cr:C}$$
$$+ y^t_{Mo}\ {}^0G^{m23c6}_{Fe:Mo:C} + y^t_V\ {}^0G^{m23c6}_{Fe:V:C}) +$$
$$y^s_{Cr}(y^t_{Fe}\ {}^0G^{m23c6}_{Cr:Fe:C} + y^t_{Cr}\ {}^0G^{m23c6}_{Cr:Cr:C}$$
$$+ y^t_{Mo}\ {}^0G^{m23c6}_{Cr:Mo:C} + y^t_V\ {}^0G^{m23c6}_{Cr:V:C}) +$$
$$RT[20(y^s_{Fe}\ln y^s_{Fe} + y^s_{Cr}\ln y^s_{Cr})$$
$$+ 3(y^t_{Fe}\ln y^t_{Fe} + y^t_{Cr}\ln y^t_{Cr} + y^t_{Mo}\ln y^t_{Mo} +$$
$$y^t_V\ln y^t_V)] + y^s_{Fe}y^s_{Cr}y^t_{Fe}y^t_{Cr}L^{m23c6}_{Fe,Cr:Fe,Cr:C}$$
$$y^s_{Fe} = y_{Fe}/(y_{Fe} + y_{Cr})$$
$$y^s_{Cr} = y_{Cr}/(y_{Fe} + y_{Cr}), \quad y^t_V = (23/3)y_V$$
$$y^t_{Mo} = (23/3)y_{Mo}, \quad y^t_{Fe} = y^s_{Fe}\,(1 - y^t_{Mo} - y^t_V),$$
$$y^t_{Cr} = y^s_{Cr}\,(1 - y^t_{Mo} - y^t_V)$$
$${}^0G^{m23c6}_{Cr:Cr:C} - 23H^{SER}_{Cr} - 6H^{SER}_C = -521{,}983$$
$$+ 3622.24T - 620.965T\ln T - 0.126431T^2$$
$${}^0G^{m23c6}_{Fe:Fe:C} - 23H^{SER}_{Fe} - 6H^{SER}_C = -5/3GHSERC$$
$$+ 23/3(-10{,}745 + 706.04T - 120.6T\ln T)$$
$$+ 66{,}920 - 40T$$
$${}^0G^{m23c6}_{V:V:C} - 23H^{SER}_V - 6H^{SER}_C = -990{,}367$$
$$+ 4330.63\,T - 728.829T\ln T + 5{,}003{,}425T^{-1}$$

$${}^0G_{\mathrm{Cr:Fe:C}} = 20/23\,{}^0G^{\mathrm{m23c6}}_{\mathrm{Cr:Cr:C}} + 3/23\,{}^0G^{\mathrm{m23c6}}_{\mathrm{Fe:Fe:C}},$$

$${}^0G^{\mathrm{m23c6}}_{\mathrm{Fe:Cr:C}} = 20/23\,{}^0G^{\mathrm{m23c6}}_{\mathrm{Fe:Fe:C}} + 3/23\,{}^0G^{\mathrm{m23c6}}_{\mathrm{Cr:Cr:C}}$$

$${}^0G^{\mathrm{m23c6}}_{\mathrm{Fe:V:C}} = 20/23\,{}^0G^{\mathrm{m23c6}}_{\mathrm{Fe:Fe:C}} + 3/23\,{}^0G^{\mathrm{m23c6}}_{\mathrm{V:V:C}}$$

${}^0G^{\mathrm{m23c6}}_{\mathrm{Fe:Mo:C}}(T)$:[16]

$${}^0G^{\mathrm{m23c6}}_{\mathrm{Fe:Mo:C}}(670\,\mathrm{K}) - 20H^{\mathrm{SER}}_{\mathrm{Fe}} - 3H^{\mathrm{SER}}_{\mathrm{Mo}} - 7H^{\mathrm{SER}}_{\mathrm{C}} = -660{,}100$$

$${}^0G^{\mathrm{m23c6}}_{\mathrm{Fe:Mo:C}}(720\,\mathrm{K}) - 20H^{\mathrm{SER}}_{\mathrm{Fe}} - 3H^{\mathrm{SER}}_{\mathrm{Mo}} - 7H^{\mathrm{SER}}_{\mathrm{C}} = -726{,}800$$

$${}^0G^{\mathrm{m23c6}}_{\mathrm{Fe:Mo:C}}(873\,\mathrm{K}) - 20H^{\mathrm{SER}}_{\mathrm{Fe}} - 3H^{\mathrm{SER}}_{\mathrm{Mo}} - 7H^{\mathrm{SER}}_{\mathrm{C}} = -949{,}460$$

${}^0G^{\mathrm{m23c6}}_{\mathrm{Cr:Mo:C}}(T)$:[16]

$${}^0G^{\mathrm{m23c6}}_{\mathrm{Cr:Mo:C}}(670\,\mathrm{K}) - 20H^{\mathrm{SER}}_{\mathrm{Cr}} - 3H^{\mathrm{SER}}_{\mathrm{Mo}} - 7H^{\mathrm{SER}}_{\mathrm{C}} = -1{,}030{,}000$$

$${}^0G^{\mathrm{m23c6}}_{\mathrm{Cr:Mo:C}}(720\,\mathrm{K}) - 20H^{\mathrm{SER}}_{\mathrm{Cr}} - 3H^{\mathrm{SER}}_{\mathrm{Mo}} - 7H^{\mathrm{SER}}_{\mathrm{C}} = -1{,}090{,}000$$

$${}^0G^{\mathrm{m23c6}}_{\mathrm{Cr:Mo:C}}(873\,\mathrm{K}) - 20H^{\mathrm{SER}}_{\mathrm{Cr}} - 3H^{\mathrm{SER}}_{\mathrm{Mo}} - 7H^{\mathrm{SER}}_{\mathrm{C}} = -1{,}284{,}035$$

${}^0G^{\mathrm{m23c6}}_{\mathrm{Cr:V:C}}(T)$:[16]

$${}^0G^{\mathrm{m23c6}}_{\mathrm{Cr:V:C}}(670\,\mathrm{K}) - 20H^{\mathrm{SER}}_{\mathrm{Cr}} - 3H^{\mathrm{SER}}_{\mathrm{V}} - 7H^{\mathrm{SER}}_{\mathrm{C}} = -827{,}000$$

$${}^0G^{\mathrm{m23c6}}_{\mathrm{Cr:V:C}}(720\,\mathrm{K}) - 20H^{\mathrm{SER}}_{\mathrm{Cr}} - 3H^{\mathrm{SER}}_{\mathrm{V}} - 7H^{\mathrm{SER}}_{\mathrm{C}} = -889{,}000$$

$${}^0G^{\mathrm{m23c6}}_{\mathrm{Cr:V:C}}(873\,\mathrm{K}) - 20H^{\mathrm{SER}}_{\mathrm{Cr}} - 3H^{\mathrm{SER}}_{\mathrm{V}} - 7H^{\mathrm{SER}}_{\mathrm{C}} = -1{,}096{,}992$$

$$L^{\mathrm{m23c6}}_{\mathrm{Fe,Cr:Fe,Cr:C}} = -252{,}350 + 80.4T$$

$\underline{\mathrm{M_6C}}$:[13,16]

Four sublattices called *s*, *t*, *u*, and *v*, sites 2:2:2:1

Constituents: Fe:Mo:Fe, Mo, Cr, V:C

$$(\mathrm{Mo}_{y_{\mathrm{Mo}}}\mathrm{Cr}_{y_{\mathrm{Cr}}}\mathrm{V}_{y_{\mathrm{V}}}\mathrm{Fe}_{y_{\mathrm{Fe}}})_6\mathrm{C} \rightarrow \mathrm{Fe_2Mo_2}(\mathrm{Mo}_{y^u_{\mathrm{Mo}}}\mathrm{Cr}_{y^u_{\mathrm{Cr}}}\mathrm{V}_{y^u_{\mathrm{V}}}\mathrm{Fe}_{y^u_{\mathrm{Fe}}})_2\mathrm{C}$$

$$\begin{aligned}\mu_{\mathrm{M_6C}} = G^{\mathrm{m6c}}_{\mathrm{m}} = {} & y^u_{\mathrm{Fe}}\,{}^0G^{\mathrm{m6c}}_{\mathrm{Fe:Mo:Fe:C}} + \\ & y^u_{\mathrm{Mo}}\,{}^0G^{\mathrm{m6c}}_{\mathrm{Fe:Mo:Mo:C}} + y^u_{\mathrm{Cr}}\,{}^0G^{\mathrm{m6c}}_{\mathrm{Fe:Mo:Cr:C}} + \\ & y^u_{\mathrm{V}}\,{}^0G^{\mathrm{m6c}}_{\mathrm{Fe:Mo:V:C}} + 2(y^u_{\mathrm{Fe}}\ln y^u_{\mathrm{Fe}} + y^u_{\mathrm{Mo}}\ln y^u_{\mathrm{Mo}} + \\ & y^u_{\mathrm{Cr}}\ln y^u_{\mathrm{Cr}} + y^u_{\mathrm{V}}\ln y^u_{\mathrm{V}}) + y^u_{\mathrm{Fe}}y^u_{\mathrm{Mo}}\,L^{\mathrm{m6c}}_{\mathrm{Fe:Mo:Fe,Mo:C}}\end{aligned}$$

$$y^u_{\mathrm{Fe}} = 3y_{\mathrm{Fe}} - 1, \quad y^u_{\mathrm{Mo}} = 3y_{\mathrm{Mo}} - 1,$$

$$y^u_{\mathrm{Cr}} = 3y_{\mathrm{Cr}}, \quad y^u_{\mathrm{V}} = 3y_{\mathrm{V}}$$

$$\begin{aligned}{}^0G^{\mathrm{m6c}}_{\mathrm{Fe:Mo:Fe:C}} - 4H^{\mathrm{SER}}_{\mathrm{Fe}} - 2H^{\mathrm{SER}}_{\mathrm{Mo}} - H^{\mathrm{SER}}_{\mathrm{C}} = {} & 4\mathrm{GHSERFE} \\ & + 2\mathrm{GHSERMO} + \mathrm{GHSERC} + 77{,}705 \\ & - 101.5T\end{aligned}$$

$$\begin{aligned}{}^0G^{\mathrm{m6c}}_{\mathrm{Fe:Mo:Mo:C}} - 2H^{\mathrm{SER}}_{\mathrm{Fe}} - 4H^{\mathrm{SER}}_{\mathrm{Mo}} - H^{\mathrm{SER}}_{\mathrm{C}} = {} & 2\mathrm{GHSERFE} \\ & + 4\mathrm{GHSERMO} + \mathrm{GHSERC} - 122{,}410 \\ & + 30.25T\end{aligned}$$

${}^0G^{\mathrm{m6c}}_{\mathrm{Fe:Mo:Cr:C}}(T)$:[16]

$${}^0G^{\mathrm{m6c}}_{\mathrm{Fe:Mo:Cr:C}}(670\,\mathrm{K}) - 2H^{\mathrm{SER}}_{\mathrm{Fe}} - 2H^{\mathrm{SER}}_{\mathrm{Mo}} - 2H^{\mathrm{SER}}_{\mathrm{Cr}} = -195{,}000$$

$${}^0G^{\mathrm{m6c}}_{\mathrm{Fe:Mo:Cr:C}}(720\,\mathrm{K}) - 2H^{\mathrm{SER}}_{\mathrm{Fe}} - 2H^{\mathrm{SER}}_{\mathrm{Mo}} - 2H^{\mathrm{SER}}_{\mathrm{Cr}} = -214{,}000$$

$${}^0G^{\mathrm{m6c}}_{\mathrm{Fe:Mo:Cr:C}}(873\,\mathrm{K}) - 2H^{\mathrm{SER}}_{\mathrm{Fe}} - 2H^{\mathrm{SER}}_{\mathrm{Mo}} - 2H^{\mathrm{SER}}_{\mathrm{Cr}} = -276{,}320$$

${}^0G^{\mathrm{m6c}}_{\mathrm{Fe:Mo:V:C}}(T)$:[16]

$${}^0G^{\mathrm{m6c}}_{\mathrm{Fe:Mo:V:C}}(670\,\mathrm{K}) - 2H^{\mathrm{SER}}_{\mathrm{Fe}} - 2H^{\mathrm{SER}}_{\mathrm{Mo}} - 2H^{\mathrm{SER}}_{\mathrm{V}} = -316{,}200$$

$${}^0G^{\mathrm{m6c}}_{\mathrm{Fe:Mo:V:C}}(720\,\mathrm{K}) - 2H^{\mathrm{SER}}_{\mathrm{Fe}} - 2H^{\mathrm{SER}}_{\mathrm{Mo}} - 2H^{\mathrm{SER}}_{\mathrm{V}} = -333{,}000$$

$${}^0G^{\mathrm{m6c}}_{\mathrm{Fe:Mo:V:C}}(873\,\mathrm{K}) - 2H^{\mathrm{SER}}_{\mathrm{Fe}} - 2H^{\mathrm{SER}}_{\mathrm{Mo}} - 2H^{\mathrm{SER}}_{\mathrm{V}} = -389{,}247$$

$$L^{\mathrm{m6c}}_{\mathrm{Fe:Mo:Fe,Mo:C}} = -37{,}700$$

Hcp ($\mathrm{M_2C}$):[13,15,16]

Two sublattices, sites 1:0.5

Constituents Mo, Cr, V, Fe:C

$$\begin{aligned}\mu_{\mathrm{MC_{0.5}}} = G^{\mathrm{hcp}}_{\mathrm{m}} = {} & y_{\mathrm{Mo}}\,{}^0G^{\mathrm{hcp}}_{\mathrm{Mo:C}} + y_{\mathrm{V}}\,{}^0G^{\mathrm{hcp}}_{\mathrm{V:C}} + \\ & y_{\mathrm{Cr}}\,{}^0G^{\mathrm{hcp}}_{\mathrm{Cr:C}} + y_{\mathrm{Fe}}\,{}^0G^{\mathrm{hcp}}_{\mathrm{Fe:C}} + \mathrm{R}T(y_{\mathrm{Mo}}\ln y_{\mathrm{Mo}} + \\ & y_{\mathrm{V}}\ln y_{\mathrm{V}} + y_{\mathrm{Cr}}\ln y_{\mathrm{Cr}} + y_{\mathrm{Fe}}\ln y_{\mathrm{Fe}}) + \\ & y_{\mathrm{Fe}}y_{\mathrm{Mo}}\,L^{\mathrm{hcp}}_{\mathrm{Fe,Mo:C}} + y_{\mathrm{Fe}}y_{\mathrm{V}}\,L^{\mathrm{hcp}}_{\mathrm{Fe,V:C}}\end{aligned}$$

$$\begin{aligned}{}^0G^{\mathrm{hcp}}_{\mathrm{Mo:C}} - H^{\mathrm{SER}}_{\mathrm{Mo}} - 0.5H^{\mathrm{SER}}_{\mathrm{C}} = {} & \mathrm{GHSERMO} \\ & + 0.5\mathrm{GHSERC} - 24{,}150 - 3.625T - 163{,}000T^{-1}\end{aligned}$$

$$\begin{aligned}{}^0G^{\mathrm{hcp}}_{\mathrm{V:C}} - H^{\mathrm{SER}}_{\mathrm{V}} - 0.5H^{\mathrm{SER}}_{\mathrm{C}} = {} & -85{,}473 + 182.441T \\ & - 30.551T\ln T - 0.00538998T^2 + 229{,}029T^{-1}\end{aligned}$$

$$\begin{aligned}{}^0G^{\mathrm{hcp}}_{\mathrm{Fe:C}} - H^{\mathrm{SER}}_{\mathrm{V}} - 0.5H^{\mathrm{SER}}_{\mathrm{C}} = {} & \mathrm{GHSERFE} + 0.5\mathrm{GHSERC} \\ & - 1462.4 + 8.282T - 1.15T\ln T \\ & + 6.4\times10^{-4}T^2 + 52{,}905 - 11.9075T\end{aligned}$$

${}^0G^{\mathrm{hcp}}_{\mathrm{Cr:C}}(T)$:[16]

$${}^0G^{\mathrm{hcp}}_{\mathrm{Cr:C}}(670\ \mathrm{K}) - H^{\mathrm{SER}}_{\mathrm{Cr}} - 0.5H^{\mathrm{SER}}_{\mathrm{C}} = -45{,}500$$

$${}^0G^{\mathrm{hcp}}_{\mathrm{Cr:C}}(720\ \mathrm{K}) - H^{\mathrm{SER}}_{\mathrm{Cr}} - 0.5H^{\mathrm{SER}}_{\mathrm{C}} = -48{,}500$$

$${}^0G^{\mathrm{hcp}}_{\mathrm{Cr:C}}(873\ \mathrm{K}) - H^{\mathrm{SER}}_{\mathrm{Cr}} - 0.5H^{\mathrm{SER}}_{\mathrm{C}} = -58{,}700$$

$$L^{\mathrm{hcp}}_{\mathrm{Fe,Mo:C}} = 13{,}030 - 33.8T,$$

$$L^{\mathrm{hcp}}_{\mathrm{Fe,V:C}} = -15{,}291 - 4.138T$$

Symbols:[12,13,15]

$$\begin{aligned}\mathrm{GHSERFE} = {}^0G^{\mathrm{bcc}}_{\mathrm{Fe:Va}} - H^{\mathrm{SER}}_{\mathrm{Fe}} = {} & 1224.83 + 124.134T \\ & - 23.5143T\ln T - 0.00439752T^2 \\ & - 5.89269\times10^{-8}T^3 + 77{,}358.5T^{-1}\end{aligned}$$

$$\begin{aligned}\mathrm{GHSERCR} = {}^0G^{\mathrm{bcc}}_{\mathrm{Cr:Va}} - H^{\mathrm{SER}}_{\mathrm{Cr}} = {} & -8851.93 + 157.48T \\ & - 26.908T\ln T + 0.00189435T^2 - \\ & 1.47721\times10^{-6}T^3 + 139{,}250T^{-1}\end{aligned}$$

$$\begin{aligned}\mathrm{GHSERMO} = {}^0G^{\mathrm{bcc}}_{\mathrm{Mo:Va}} - H^{\mathrm{SER}}_{\mathrm{Mo}} = {} & -7747.247 + 131.9197T \\ & - 23.56414T\ln T - 0.003443396T^2 \\ & + 5.662834\times10^{-7}T^3 - 1.309256 \\ & \times10^{-10}T^4 + 65812.39T^{-1}\end{aligned}$$

$$\begin{aligned}\mathrm{GHSERV} = {}^0G^{\mathrm{bcc}}_{\mathrm{V:Va}} - H^{\mathrm{SER}}_{\mathrm{V}} = {} & -7930.43 + 133.346053T \\ & - 24.134T\ln T - 0.003098T^2 + 1.2175 \\ & \times10^{-7}T^3 + 69{,}460T^{-1} \\ & \text{for } 298.15 < T < 790\,\mathrm{K}\end{aligned}$$

$$\begin{aligned}\mathrm{GHSERV} = {}^0G^{\mathrm{bcc}}_{\mathrm{V:Va}} - H^{\mathrm{SER}}_{\mathrm{V}} = {} & -7967.842 + 143.291093T \\ & - 25.9T\ln T + 6.25\times10^{-5}T^2\end{aligned}$$

$$- 6.8 \times 10^{-7} T^3 \qquad \text{for } 790 < T < 2183\,\text{K}$$

$$\begin{aligned}\text{GHSERC} = {}^0G_{\text{C}}^{\text{gra}} - H_{\text{C}}^{\text{SER}} &= -17{,}369 + 170.73T \\ &- 24.3T \ln T - 4.723 \times 10^{-4} T^2 \\ &+ 2{,}562{,}600 T^{-1} - 2.643 \times 10^8 T^{-2} \\ &+ 1.2 \times 10^{10} T^{-3}.\end{aligned}$$

ACKNOWLEDGMENTS

We are grateful for the insightful discussions with S. van der Zwaag on the physicochemical aspects of methane formation. We also acknowledge fruitful discussions with P. Manolatos and H. van Wortel. The work of SMS was supported through the Brite-Euram project BE 1835 Prediction of Pressure Vessel Integrity in Creep Hydrogen Service.

REFERENCES

1. P.G. Shewmon: *Metall. Trans. A*, 1976, vol. 7A, pp. 279-86.
2. P.G. Shewmon: *Mater. Sci. Technol.*, 1985, vol. 1, pp. 2-11.
3. T.A. Parthasarathy: *Acta Metall.*, 1985, vol. 33, pp. 1673-81.
4. G. Sundararajan and P.G. Shewmon: *Metall. Trans. A*, 1981, vol. 12A, pp. 1761-75.
5. T. Nomura and T. Sakai: *ASME Pressure Vessel & Piping Conf. 97*, July 27–31, 1997, Orlando, FL, ASME, Fairfield, NJ, pp. 315-24.
6. T.A. Parthasarathy and P.G. Shewmon: *Metall. Trans. A*, 1984, vol. 15A, pp. 2021-27.
7. B.L. Chao, G.R. Odette, and G.E. Lucas: "Kinetics and Mechanisms of Hydrogen Attack in 2.25Cr-1Mo Steel," ONRI/Sub/82-22276/01, University of California, Santa Barbara, CA, Aug. 1988.
8. M.W.D. van der Burg, E. van der Giessen, and R.C. Brouwer: *Acta Mater.*, 1996, vol. 44, pp. 505-18.
9. R. Lundberg, M. Waldenstrom, and B. Uhrenius: *CALPHAD*, 1977, vol. 1, pp. 159-99.
10. M. Hillert and L.-I. Staffansson: *Acta Chem. Scand.*, 1970, vol. 24, pp. 3618-26.
11. B. Sundman and J. Agren: *J. Phys. Chem. Solids*, 1981, vol. 42, pp. 297-301.
12. J.-O. Andersson: *Metall. Trans. A*, 1988, vol. 19A, pp. 627-36.
13. J.-O. Andersson: *CALPHAD*, 1988, vol. 12, pp. 9-23.
14. W. Huang: *Z. Metallkd.*, 1991, vol. 82, pp. 391-401.
15. W. Huang: *Metall. Trans. A*, 1991, vol. 22A, pp. 1911-20.
16. *MTDATA: Metallurgical and Thermochemical Databank*, National Physical Laboratory, Teddington, Middlesex, United Kingdom, 1995.
17. H.-M. Shih and H.H. Johnson: *Acta Metall.*, 1982, vol. 30, pp. 537-45.
18. P.G. Shewmon: *Acta Metall.*, 1987, vol. 35, pp. 1317-24.
19. G.R. Odette and S.S. Vagarali: *Metall. Trans. A*, 1982, vol. 13A, pp. 299-303.
20. M. Hillert and M. Jarl: *CALPHAD*, 1978, vol. 2, pp. 227-38.
21. A. Kroupa, A. Vyrostkova, M. Svoboda, amd J. Janovec: *Acta Mater.*, 1998, vol. 46, pp. 39-49.
22. M.W.D. van der Burg and E. van der Giessen: *Acta Mater.*, 1997, vol. 45, pp. 3047-57.
23. R.L. Klueh: *J. Nucl. Mater.*, 1974, vol. 54, pp. 41-51.
24. D. Hull and D.E. Rimmer: *Phil. Mag.*, 1959, ser. 8, vol.4, pp. 673-87.
25. E. van der Giessen, M.W.D. van der Burg, A. Needleman, and V. Tvergaard: *J. Mech. Phys. Solids*, 1995, vol. 43, pp. 123-65.
26. T.A. Parthasarathy, H.F. Lopez, and P.G. Shewmon: *Metall. Trans. A*, 1985, vol. 16A, pp. 1143-49.
27. P. Schwarzkopf and R. Kiefer: *Refractory Hard Metals*, The Macmillan Company, New York, NY, 1953, pp. 104-37.
28. H. Lopez and P.G. Shewmon: *Acta Metall.*, 1983, vol. 31, pp. 1945-50.
29. P. Manolatos: Joint Research Center, Petten, The Netherlands, unpublished research, 1999.
30. H.J. Frost and M.F. Ashby: *Deformation-Mechanism Maps*, 1st ed., Pergamon Press, Oxford, United Kingdom, 1982, pp. 62-63.
31. M.W.D. van der Burg and E. van der Giessen: *Mater. Sci. Eng. A*, 1996, vol. 220, pp. 200-14.